BMC Oral Health

RESEARCH

Open Access

Efficacy of two radiographic algorithms for detection of peri-implant bone defects on cone-beam computed tomography scans

Faezeh Yousefi[1], Ali Heidari[5], Azita Ehsani[2*], Maryam Farhadian[3] and Marzieh Ehsani[4]

Abstract

Background Early detection of peri-implant bone defects can improve long-term durability of dental implants. By the advances in cone-beam computed tomography (CBCT) scanners and introduction of new algorithms, it is important to find the most efficient protocol for detection of bone defects. This study aimed to assess the efficacy of metal artifact reduction (MAR) and advanced noise reduction (ANR) algorithms for detection of peri-implant bone defects.

Materials and methods In this in vitro study, 40 titanium implants were placed in 7 sheep mandibles. Crestal, apical, and Full defects ($n=10$ from each type) were created around the implants, and 10 implants were also placed as controls. CBCT scans were obtained in four modes: with MAR, with ANR, with both MAR and ANR, and without any filter. Totally, 28 scans were obtained and evaluated by a radiologist and a maxillofacial surgeon. The observers recorded their observations in a checklist, and data were analyzed by SPSS version 21 using the kappa coefficient of agreement, sensitivity and specificity values, area under the receiver operating characteristic (ROC) curve (AUC), intraclass correlation coefficient, t-test and paired t-test ($P<0.05$).

Results The inter-observer agreement was high for detection of all defects in all modes except with ANR. No significant difference was found in AUC and diagnostic accuracy of different scan modes ($P>0.05$). The most common diagnostic error was related to misdiagnosis of control group with full defect with ANR filter, such that the existing bone was not detected. Defect depth was averagely over-estimated while defect length was under-estimated. Correct diagnosis of defects had the highest frequency when both filters were on.

Conclusion The diagnostic accuracy and sensitivity for detection of different defect types were not significantly different in different scan modes but activation of ANR filter significantly decreased the specificity and positive predictive value compared with no use of filter.

Keywords Cone-Beam Computed Tomography, Bone defect, Dental implants, Advanced noise reduction, Metal artifact reduction

*Correspondence:
Azita Ehsani
a.ehsani92@gmail.com
Full list of author information is available at the end of the article

Background

Periimplantitis is an inflammatory condition that leading to destruction of peri- implant bone and soft tissue inflammation based on its severity. Lack of enough bone around implant increases the risk of peri- implant mucositis, periimplantitis and peri- implant bone defects like dehiscence and fenestration [1]. Early accurate radiographic evaluation of bone defects around dental implants is crucial because the extension and shape of surrounding bone have an important role in prognosis of periimplantitis treatment [2]. Diagnostic imaging is used as a guiding method for assessment of alveolar bone height and detection of bone defects. Imaging modalities used for detection and evaluation of bone defects include the intraoral radiography, panoramic radiography, computed tomography, and cone-beam computed tomography (CBCT) [3, 4].

Intraoral radiographic modalities are conventionally used for assessment of implant site after implant placement. Nonetheless, they may not provide sufficient information for detection of peri-implant dehiscence when changes are insignificant or defects are in the buccal or lingual bone plates due to two-dimensional nature of images and superimposition of adjacent structures [5].

CBCT is currently used for diagnostic purposes. It has high accuracy and quality, and provides three-dimensional (3D) images with no distortion that allow precise assessment of bone defects in axial, sagittal, coronal, and cross-sectional planes [4, 6, 7].

Beam hardening and streaking artifacts are the main limitations of CBCT scanners in dental implant imaging, which can adversely affect correct diagnosis and treatment planning [8]. The metal artifact reduction (MAR) algorithm improves the image quality by applying a mathematical algorithm on the raw data after the scanning process and during image reconstruction. MAR has different algorithms, and several strategies may be used for classification of different methods of MAR, such as irradiation-dependent method, image-dependent method, and combined method. Although the mechanism of MAR algorithms has not been clearly disclosed, the MAR algorithms recently used in scanners operate based on the projection completion method, which means that the lost values are calculated by averaging the adjacent pixels [9].

Some CBCT scanners are equipped with adaptive imaging noise optimizer (AINO). AINO analyzes the exposure information and differentiates between noise and fine details during image reconstruction, resulting in improvement of image quality by noise reduction. Noise is an inherent property of scans that use very small voxel sizes. The advanced noise reduction (ANR) algorithm which is available in some CBCT devices, decreasing the noise of images [10]. By the recent advances in CBCT scanners and 3D reconstructions, availability of different sizes of fields of view, and introduction of new software programs, it is important to find the most efficient scanner and settings for early detection of bone defects. Since no precise information is available regarding the simultaneous effect of these algorithms on the diagnostic quality of images, this study aimed to assess the effect of activation of both ANR and MAR algorithms of Kodak Carestream CS9600 CBCT device on detection of peri-implant bone defects for the first time.

Materials and methods

This in vitro experimental study was carried out after obtaining ethical approval from the ethics committee of Hamadan University of Medical Sciences (IR.UMSHA.REC.1401 – 671). In this study, seven sheep were sacrificed in accordance with Islamic slaughtering practices, and heads of sheep were used. Forty titanium dental implants (SIC invent AG, Switzerland) with 4 mm diameter and 10 mm length were placed in 7 sheep mandibles with soft tissue by an experienced oral and maxillofacial surgeon.

For insertion of implants, a pilot drill was initially used for osteotomy and drilling was continued by using consecutive drills according to implant size (4×10 mm). Then implants were inserted at low speed (40 rpm) with maximum torque (40 N/cm) such that the implant crest was at the level of the buccal bone crest.

After that, simulated Crestal bone defect group (CBD), Apical bone defect group (ABD) and Full bone defect group (FBD) were artificially created in the buccal bone plates [11]. CBD had 5 mm length starting from the implant crest and with 2 mm depth (from buccal wall to the implant external surface (Fig. 1). ABD was created in the bone adjacent to the apical third of the dental implant and had 5 mm length (between two edge of bone) and 2 mm depth. FBD had 10 mm length and 2 mm depth. (Figures 2, 3, 4 and 5) Also, the width of all defects was equal to the implant width (distance between the mesial and distal implant surfaces. The defects were created by using a surgical hand-piece (X65L TI, NSK, Japan) and ¼ and ½ cylindrical carbide burs (KG Sorensen, Zenith Dental Aps, Agerskov, Denmark) at high speed under saline irrigation. The size of defects created around dental implants was measured by a caliper to serve as the gold standard. Ten implants were placed for each type of defects (overally 30 implants) and ten implants inserted as the Control group (Ctl) with no defect.

After creation of defects, all defective areas were recorded without the knowledge of the observers. The soft tissue was then sutured, and the mandibles were prepared for imaging.

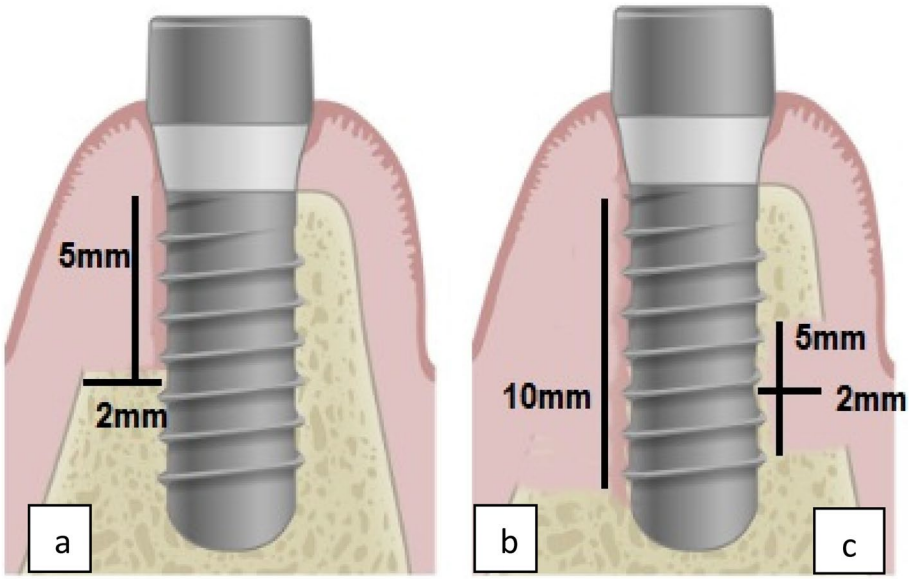

Fig. 1 Schematic picture of **a**:CBD, **b**:FBD and **c**:ABD,respectively

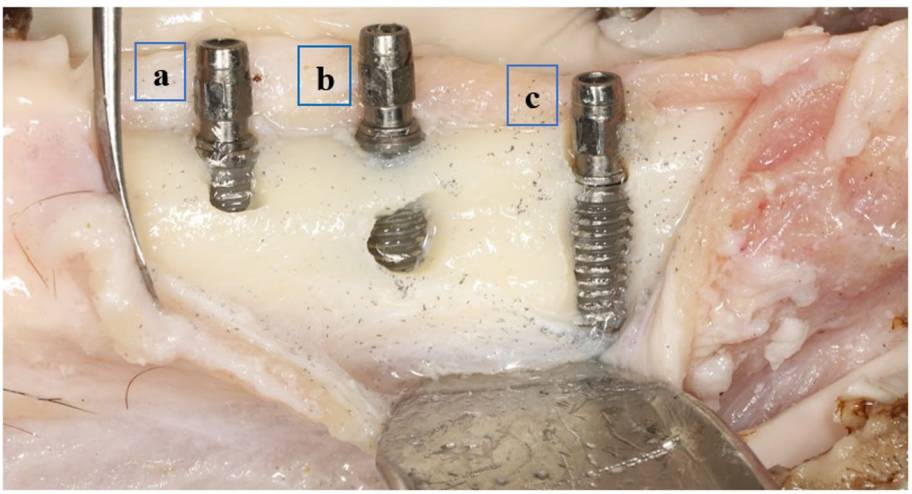

Fig. 2 Defects from the buccal view (**a**: crestal defect, **b**: apical defect, **c**: full defect)

Scans were obtained using Kodak CS9600 (Carestream Health, Trophy, France) CBCT scanner at the School of Dentistry of Hamadan University of Medical Sciences. The exposure settings included 90 kvp, 10 mA, 10 s of exposure time, 150 µm voxel size, and 8×8 cm field of view. All mandibles were scanned after activation of four scan modes (ANR, MAR, Both (ANR&MAR) and None) so totally 28 scans were captured. The images were stored in OnDemand software (Cybermed, Seoul, South Korea). One oral radiologist and one oral and maxillofacial surgeon viewed the reformatted panoramic and cross-sectional images on a 20-inch monitor (LG, Seoul, South Korea) under standard conditions. Slice thickness and slice interval were chosen by the observers and other orthogonal planes and images with different slice thicknesses were also used if required by the observers. The observers evaluated the peri-implant and length and depth of buccal bone defect adjacent to each implant were recorded in a checklist. Defect length was measured as the vertical distance from beneath the crest module to the apical base of the defect. Defect depth was recorded as the distance from the buccal wall to the external implant surface at the middle height of the defect. Also, 20% of the images were evaluated again by the same

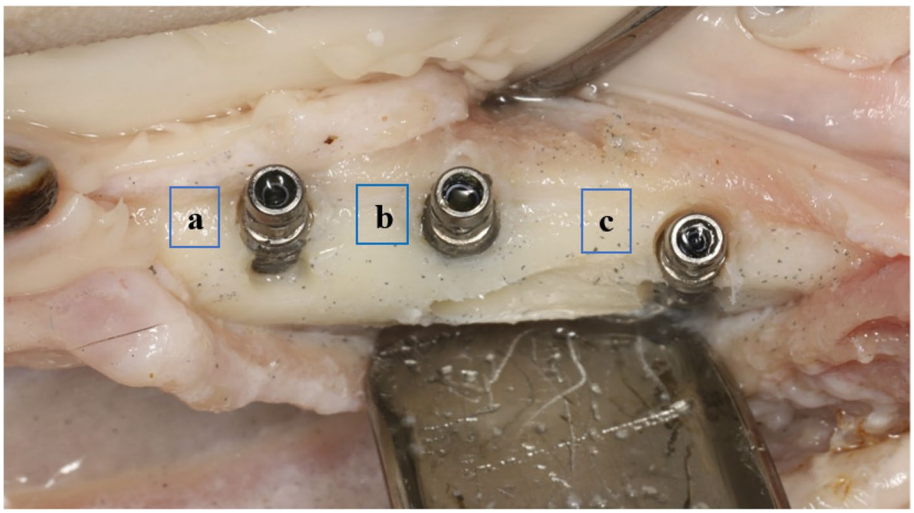

Fig. 3 Defects from the occlusal view (**a**: crestal defect, **b**: apical defect, **c**: full defect)

observers after a 2-week interval to assess intra-observer agreement.

Statistical analysis

The collected data were analyzed by SPSS version 21 using descriptive and analytical statistics including the kappa coefficient of agreement, sensitivity, specificity, area under the receiver operating characteristic (ROC) curve (AUC), intraclass correlation coefficient, t-test and paired t-test at 0.05 level of significance.

Results

A total of 30 bone defects (10 apical, 10 crestal, and 10 full) with equal distribution were artificially created in 7 freshly slaughtered sheep mandibles. Table 1 presents the inter- and intra-observer agreements for each of the four scan modes. As shown, the inter-observer agreement (calculated by the kappa coefficient) was the highest when no filter was used (0.89). The intra-observer agreement ranged from 0.50 to 0.90, and the lowest value was recorded following the activation of ANR.

Tables 2 and 3 show the accuracy, sensitivity, specificity and positive (PPV) and negative (NPV) predictive values for detection of bone defects in different scan modes and their comparison for each observer.

As shown in Table 2, The lowest accuracy was recorded when the MAR filter was active (0.73 ± 0.1). Sensitivity, which indicates correct detection of defects, was the highest when both filters were on (0.70 ± 0.17). Specificity, which indicates correct detection of sound (defect-free) areas, was 100% when no filter was on, and equal to the value when both filters were on.

As shown in Table 3, The lowest accuracy was recorded when the ANR filter was on and the highest was recorded when the MAR filter was on (0.9 ± 0.08) which was in contrast with Table 2. (0.8 ± 0.13). Sensitivity and Specificity was the highest when MAR filter was on.

Depth and length of defects measured by the observers are shown in Table 4.

As shown in Table 4 regarding the length and depth of crestal defects reported by the observers, defect depth (2 mm) was over-estimated in all cases. For the first observer, a significant difference was found in the estimated value between the use and no use of filters ($P < 0.05$), such that activation of filters resulted in significant over-estimation of defect depth. The length of crestal defects was under-estimated in all cases.

The apical defect depth was over-estimated in all cases. The most accurate values were recorded by the observers when the MAR filter was on. Apical defect length was under-estimated in all cases. The most accurate values were recorded by the observers when both filters were on (mean diff.=−0.05). No significant difference was found among different scan modes.

The full defect length was underestimated in all cases, which was the same as the results regarding apical and crestal defect lengths. A significant difference was found between the recorded defect length and the gold standard when the MAR filter and both filters were on.

Discussion

Post-surgical peri-implant bone loss can occur due to incorrect implant placement, or excessive load application. Faster detection of such defects and their treatment are important to prevent esthetic complications, and

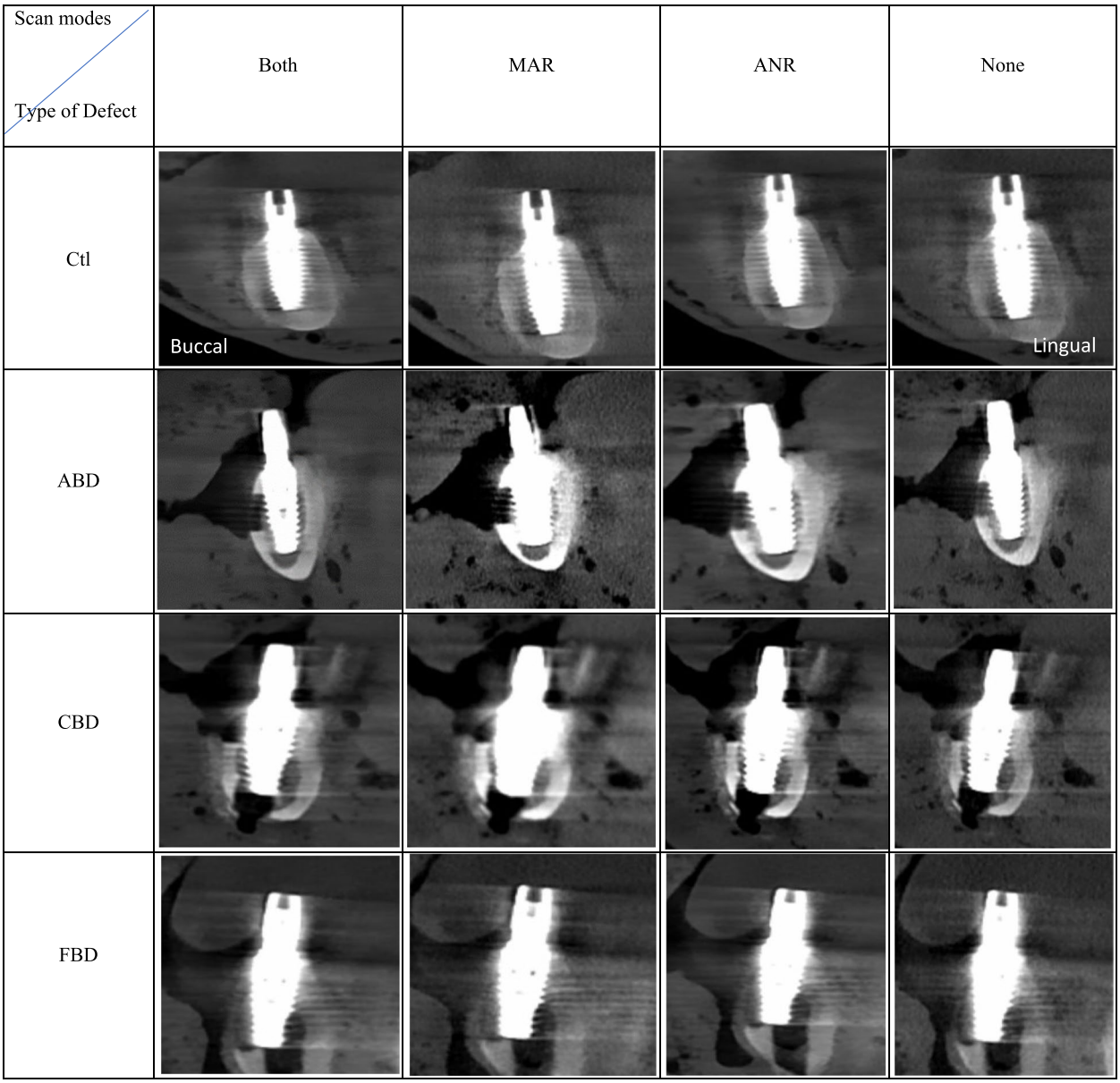

Fig. 4 Shows CBCT images of the control group and different defect types in the four scan modes

improve oral hygiene and durability of dental implants [12]. Defects in areas other than the inter-proximal area (buccal and lingual) may be masked on the conventional two-dimensional radiographs due to superimposition of anatomical structures. Thus, CBCT may be the best imaging modality for assessment of buccal and palatal bone plates and better observation of bone morphology [3]. A precise and reliable imaging modality is imperative for assessment of crestal bone level and peri-implant defects. In studies done before [3, 13] peri- implant defects are assessed in dry human mandibles or bovine ribs. In this situation, as there is only bone and we have no soft tissue, recognition of bone defects would be easier. But in the oral cavity in real situation, we have both hard and soft tissue that the detection of defects would be much more complicated. Because of this issue we decided to use the slaughtered sheep mandibles to simulate both hard and soft tissue that would be more resemble to the real environment that is exist in the oral cavity. So, we think it could be a superiority of this manuscript to the researches that have done before. Also, In this study similar to other researches we created defects on buccal surface of alveolar ridge because it is more prone to bone loss due to its low thickness [14].

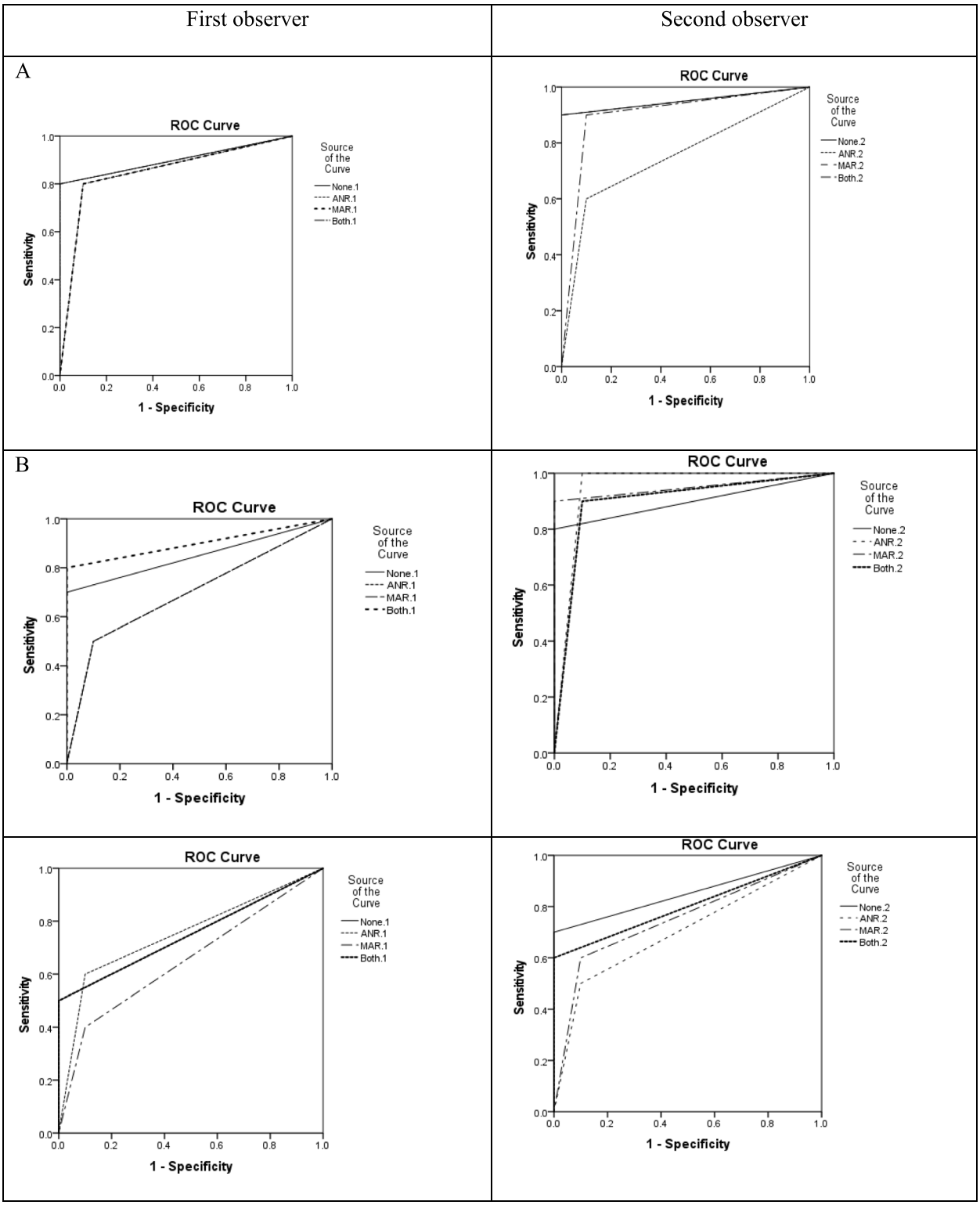

Fig. 5 Shows the ROC curves of the three defect types for the two observers in four scan modes. As shown, a larger AUC indicates better performance of the observer in the respective mode

Table 1 Intra- and inter-observer agreements in different scan modes

Scan mode	Inter-observer (kappa (SE	*P* value	Intra-observer (weighted kappa (SE))			
			Observer 1		Observer 2	
			kappa (SE)	*P* value	kappa (SE)	*P* value
None	(099.0) 89.0	001.0>	(131.0) 80.0	001.0>	(097.0) 90.0	001.0>
ANR	(180.0) 58.0	007.0	(159.0) 70.0	002.0	(185.0) 50.0	019.0
MAR	(135.0) 79.0	001.0>	(159.0) 70.0	002.0	(097.0) 90.0	001.0>
Both	(131.0) 80.0	001.0>	(131.0) 80.0	001.0>	(134.0) 80.0	001.0>

Table 2 Accuracy, sensitivity, specificity, PPV and NPV for detection of bone defects in different scan modes by the first observer and their comparison

Scan modes		Accuracy		Sensitivity		Specificity		PPV		NPV	
		Mean±SD	*P* *	Mean±SD	*P* *	Mean±SD	*P* *	Mean±SD	*P* *	Mean±SD	*P* *
None	None-ANR	0.07±0.83	0.26	0.66±0.15	0.82	0.00±1.00	**0.03**	0.00±1.00	**0.03**	0.08±0.75	0.51
ANR		0.07±0.76		0.15±0.63		0.04±0.92		0.02±0.85		0.08±0.71	
None	None MAR	0.07±0.83	0.18	0.66±0.15	0.5	0.00±1.00	**0.02**	0.00±1.00	**0.03**	0.08±0.75	0.27
MAR		0.10±0.73		0.20±0.56		0.00±0.9		0.04±0.83		0.11±0.68	
None	None-Both	0.07±0.83	0.63	0.66±0.15	0.63	0.00±1.00	1	0.00±1.00	1	0.08±0.75	0.63
Both		0.08±0.85		0.70±0.17		0.00±1.00		0.00±1.00		0.09±0.77	
ANR	ANR-MAR	0.07±0.76	0.5	0.15±0.63	0.5	0.04±0.92	0.3	0.02±0.85	0.5	0.08±0.71	0.5
MAR		0.10±0.73		0.20±0.56		0.00±0.9		0.04±0.83		0.11±0.68	
ANR	ANR-Both	0.76±0.76	0.17	0.15±0.63	0.63	0.04 ±0.92	**0.03**	0.02±0.85	**0.03**	0.08±0.71	0.26
Both		0.08±0.85		0.70±0.17		0.00±1.00		0.00±1.00		0.09±0.77	
MAR	MAR-Both	0.10±0.73	0.12	0.20±0.56	0.34	0.00±0.9	**0.02**	0.04±0.83	**0.03**	0.11±0.68	0.12
Both		0.08±0.85		0.70±0.17		0.00±1.00		0.00±1.00		0.09±0.77	

*Statistical tested: t-test. *p* value less than 0.05 shows statistical significance

Table 3 Accuracy, sensitivity, specificity, PPV and NPV for detection of bone defects in different scan modes by the second observer and their comparison

Scan modes		Accuracy		Sensitivity		Specificity		PPV		NPV	
		Mean ± SD	*P* *	Mean ± SD	*P* *	Mean ± SD	*P* *	Mean ± SD	*P* *	Mean ± SD	*P* *
None-ANR	None	0.05 ± 0.9	0.37	0.8 ± 0.10	0.51	0.00 ± 1.00	**0.02**	0.00 ± 1.00	**0.03**	0.07 ± 0.83	0.51
	ANR	0.13 ± 0.8		0.26 ± 0.7		0.00 ± 0.9		0.03 ± 0.86		0.19 ± 0.77	
None-MAR	None	0.05 ± 0.9	0.81	0.8 ± 0.10	0.81	0.00 ± 1.00	1.00	0.00 ± 1.00	1.00	0.07 ± 0.83	0.81
	MAR	0.08 ± 0.9		0.17 ± 0.8		0.00 ± 1.00		0.00 ± 1.00		0.10 ± 0.83	
None-Both	None	0.05 ± 0.9	0.48	0.8 ± 0.10	0.81	0.00 ± 1.00	**0.02**	0.00 ± 1.00	**0.03**	0.07 ± 0.83	0.81
	Both	0.08 ± 0.85		0.8 ± 0.17		0.00 ± 0.9		0.02 ± 0.88		0.12 ± 0.83	
ANR-MAR	ANR	0.13 ± 0.8	0.24	0.26 ± 0.7	0.65	0.00 ± 0.9	**0.02**	0.03 ± 0.86	**0.03**	0.19 ± 0.77	0.50
	MAR	0.08 ± 0.9		0.17 ± 0.8		0.00 ± 1.00		0.00 ± 1.00		0.10 ± 0.83	
ANR-Both	ANR	0.13 ± 0.8	0.65	0.26 ± 0.7	0.65	0.00 ± 0.9	1.00	0.03 ± 0.86	0.34	0.19 ± 0.77	0.65
	Both	0.08 ± 0.85		0.8 ± 0.17		0.00 ± 0.9		0.02 ± 0.88		0.12 ± 0.83	
MAR-Both	MAR	0.08 ± 0.9	0.26	0.17 ± 0.8	1.00	0.00 ± 1.00	**0.02**	0.00 ± 1.00	**0.03**	0.10 ± 0.83	0.79
	Both	0.08 ± 0.85		0.8 ± 0.17		0.00 ± 0.9		0.02 ± 0.88		0.12 ± 0.83	

*Statistical tested: t-test. *p* value less than 0.05 shows statistical significance

Table 4 Size of Crestal, apical and full apical defects measured by the observers in different scan modes

Groups	Scan Modes	Measurement Type	Observer 1			Observer 2		
			Mean ± SD	Mean Diff	*P**	Mean ± SD	Mean Diff	*P**
CBD	**None**	**Depth**	2.56 ± 0.55	0.65	0.35	2.25 ± 0.52	0.25	0.17
		Length	3.48 ± 0.68	−1.51	0.00	4.09 ± 0.43	−0.9	> 0.001
	ANR	**Depth**	2.67 ± 0.54	0.67	0.01	2.16 ± 0.46	0.16	0.29
		Length	4.14 ± 0.66	−0.85	0.01	4.09 ± 0.43	−0.77	0.00
	MAR	**Depth**	2.46 ± 0.32	0.46	0.02	2.22 ± 0.44	0.22	0.14
		Length	3.60 ± 1,02	−1.39	0.03	4.51 ± 0.69	−0.48	0.05
	Both	**Depth**	2.56 ± 0.43	0.56	0.00	2.03 ± 0.25	0.03	0.67
		Length	3.84 ± 0.98	−1.15	0.01	4.31 ± 0.72	−0.69	0.01
ABD	**None**	**Depth**	2.66 ± 0.62	0.66	0.13	2.37 ± 0.45	0.37	0.14
		Length	4.53 ± 1.14	−0.46	0.26	4.44 ± 1.27	−0.5	0.79
	ANR	**Depth**	2.56 ± 0.47	0.56	0.00	2.47 ± 0.38	0.47	0.19
		Length	4.93 ± 1.25	−0.06	0.88	4.77 ± 2.64	−0.23	0.06
	MAR	**Depth**	2.48 ± 0.4	0.48	0.00	2.26 ± 0.42	0.26	0.00
		Length	4.59 ± 0.8	−0.4	0.17	4.24 ± 1.56	−0.76	0.62
	Both	**Depth**	2.58 ± 0.47	0.58	0.00	2.34 ± 0.37	0.34	0.02
		Length	4.66 ± 1.13	−0.33	0.4	4.95 ± 1.66	−0.05	0.96
FBD	**None**	**Length**	8.37 ± 3.22	−1.62	0.23	8.48 ± 2.38	−1.51	0.11
	ANR	**Length**	7.32 ± 1.88	−2.67	0.00	7.81 ± 2.4	−2.18	0.05
	MAR	**Length**	7.61 ± 2.79	−2.38	0.06	7.83 ± 2.11	−2.16	0.03
	Both	**Length**	7.39 ± 2.2	−2.6	0.00	7.78 ± 2.16	−2.21	0.03

*Statistical tested: Paired t-test. *p* value less than 0.05 shows statistical significance

CBD Crestal bone defect, *ABD* Apical bone defect, *FBD* Full bone defect

Information about image enhancement filters is limited. Some authors reported that MAR and ANR image enhancement filters of CBCT improved the image quality during image reconstruction [15]. The MAR algorithm increases the contrast to noise ratio and decreases the interferences caused by opaque objects such as metals on the images. Nonetheless, the efficacy of the MAR algorithm depends on the CBCT scanner manufacturer [16]. Thus, the present study aimed to assess the efficacy of MAR and ANR filters of CS9600 Carestream CBCT scanner for detection of peri-implant defects in sheep mandible with soft tissue.

Three types of defects were created in the present study. The crestal defects were similar to dehiscence defects while the apical defects were similar to fenestration defects. Full defects were also created, which have not been evaluated in any previous study; however, they occur in the clinical setting. Full defects start from the implant crest and extend to the apical region, and are more commonly seen in implant placement for cases with a thin buccal plate when the implant almost adheres to the wall.

Differentiation between artifacts caused by opaque objects and peri-implant bone loss is a challenge, especially when it compromises the correct detection of bone level and results in false positive and false negative results.

However, the CBCT scans of defects show hypodense and irregular areas surrounded by hyperdense areas (due to the presence of residual bone trabeculae). This pattern can help in differentiation between these areas and peri-implant artifacts that are completely hypodense and have a more regular border. Kamburoglu et al. [13]evaluated the diagnostic accuracy for detection of peri-implant buccal dehiscence with and without the MAR algorithm and found no significant difference between the two modes.

Bechara et al. [17] reported the effects of MAR on contrast to noise ratio (CNR)and recommended its activation to obtain high-quality images. In another study, Bechara et al. [18], evaluated the effect of activation of MAR on detection accuracy of two CBCT scanners for root fracture in endodontically treated teeth and reported higher diagnostic accuracy when MAR was not used.

Freire et al. [19] evaluated the effect of a metal artifact reduction algorithm on dehiscence and fenestration detection around zirconia implants. Zirconia implants cause extremely strong artifacts in CBCT images and MAR algorithm did not significantly affect peri-implant defects detection around these implants.

Similarly in the present study, the accuracy, sensitivity, and specificity of detection of all defect types were lower when the MAR filter was on, compared with no application of any filter but the difference did not reach statistical significance.

In fact, application of MAR in CBCT, decreases the mean gray value and subsequently the standard deviation of the gray value. However, it cannot be stated with certainty that application of MAR increases the Contrast to noise ratio. Apparently, CNR is affected by some other parameters such as tube potential (Kvp), tube current (mA), voxel size, and implant site as well [20]. Resultantly, literature is controversial regarding the efficacy of application of the MAR algorithm.

Parrone et al. [10] evaluated the effect of AINO on detection of vertical root fracture in endodontically treated teeth and reported no significant improvement in diagnostic accuracy. Consistent with their results, the present study showed the lowest accuracy and sensitivity in detection of all types of defects when the ANR filter was on; however, the difference with other scan modes was not significant. But specificity and positive predictive value significantly decreased when the ANR filter was on. This finding may be due to the fact that the highest efficacy of ANR filter in large fields of view is due to reduction of noise, and it decreases the accuracy of detection of details in small fields of view.

In the present study, the observers also recorded the size of different defect types. Defect length (5 and 10 mm) was under-estimated in all cases. The most accurate size was recorded by the observers when both filters were on; but no significant difference was found among different scan modes in this regard. Defect depth (2 mm) was over-estimated in all cases. A significant difference was noted in the estimated defect depth by the first observer when filters were on compared with their off mode, such that activation of filters resulted in significant over-estimation of defect depth.

Under in vitro conditions, the accuracy of CBCT for measuring the defect size is significantly affected by the size of defect and presence of artifacts [16]. Kamburoglu et al. [21] created several dehiscence defects with variable sizes around dental implants in dry human mandibles. They classified the defects based on their length and depth into three groups of small (1–3 mm), medium (3–5 mm), and large (>5 mm). Small defects had lower diagnostic accuracy than medium and large defects. Their results were in agreement with the findings of Hilgenfeld et al. [22] and Pinheiro et al. [23] that reported an improvement in detection accuracy by an increase in defect size. In the present study, however, the defect size was the same due to high number of variables evaluated.

In a study by Schwindling et al. [24], the beam hardening artifact complicated the measurement of defect depth; nonetheless, the measured defect width matched the gold standard (actual value). The same was reported by Kamburoglu et al. [21] They concluded that the mean deviation values were higher for defect depth.

The reason was that in most cases, the deepest part of the defect is completely adjacent to the implant, and thus, the amount of artifacts would be higher in this area [24]. However, a definite judgment cannot be reached in this regard since different CBCT scanners have different voxel sizes and fields of view, which along with patient position can affect the results [25].

Furthermore, it should be noted that the soft tissue, bone, dental structure, and beam hardening artifacts caused by opaque structures can all affect the signal to noise ratio and subsequently the image quality. Moreover, artifact reduction algorithms have been designed for use on living individuals in the clinical setting. Thus, artifacts see in animal models may be different from what actually occurs in the clinical setting. One strength of the present study was placement of several implants in each quadrant of sheep mandibles to assess the efficacy of algorithms in presence of several dental implants next to each other. Small sample size due to limitations in CBCT, in vitro design, not considering motion artifacts, use of only one CBCT scanner and one specific imaging protocol, and also dissimilarity of sheep soft tissue and human soft tissue were among the limitations of the present study. Future studies are recommended on different CBCT scanners with different exposure parameters and fields of views on a larger sample size, and with higher number of observers and higher frequency of observations to obtain more accurate results. Also, artificial intelligence and deep learning algorithms may be used for artifact reduction.

Conclusion

The diagnostic accuracy and sensitivity of detection of defect types were not significantly different in different scan modes but activation of the ANR filter significantly decreased the specificity and positive predictive value compared with no application of filters.

According to the present results, the highest frequency of correct detection of defects was recorded when both filters were on. The most common diagnostic error was related to misdiagnosis of control group with full defect when the ANR filter was on, such that the existing bone was not detected.

Abbreviations

CBCT Cone Beam Computed Tomography
MAR Metal Artifact Reduction
ANR Advanced Noise Reduction

Acknowledgements
This study was part of MD thesis in maxillofacial radiology (thesis number:140109017208),which was supported by the Vice-Chancellor of Research and Technology, Hamadan university of Medical Science, Hamadan, Iran.

Authors' contributions
The authors confirm contribution to the paper as follows: study conception and design :A.E,F.Y,A.H; Perform Surgery :A.E,A.H .data collection: A.E; analysis and interpretation of results: M.F; draft manuscript preparation: F.Y,A.E. Writing–review & editing: M.E. All authors reviewed the results and approved the final version of the manuscript.

Funding
This study was funded by Hamadan University of Medical Sciences as a part of MD thesis.

Data availability
The datasets used and/or analysed during the current study are available from the corresponding author on reasonable request.

Declarations

Ethics approval and consent to participate
This in vitro experimental study was carried out after obtaining ethical approval from the ethics committee of Hamadan University of Medical Sciences (IR.UMSHA.REC.1401 – 671(.

Consent for publication
Not applicable.

Competing interests
The authors declare no competing interests.

Author details
[1]Department of Oral and Maxillofacial Radiology, Dental Research Center, Hamadan University of Medical Sciences, Hamadan, Iran. [2]Department of Oral and Maxillofacial Radiology, School of Dentistry, Alborz University of Medical Sciences, Karaj, Iran. [3]Dental Implants Research Center, School of Public Health and Research Center for Health Sciences, Hamadan University of Medical Sciences, Hamadan, Iran. [4]Resident of Oral and Maxillofacial Radiology, Isfahan University of Medical Sciences, Isfahan, Iran. [5]Department of Oral and Maxillofacial Surgery, Dental Research Center, Hamadan University of Medical Science, Hamadan, Iran.

Received: 25 June 2024 Accepted: 26 December 2024
Published online: 07 January 2025

References

1. Nomier AS, Gaweesh YSE-D, Taalab MR, El Sadat SA. Efficacy of low-dose cone beam computed tomography and metal artifact reduction tool for assessment of peri-implant bone defects: an in vitro study. BMC Oral Health. 2022;22(1):1–11.
2. Dave M, Davies J, Wilson R, Palmer R. A comparison of cone beam computed tomography and conventional periapical radiography at detecting peri-implant bone defects. Clin Oral Implants Res. 2013;24(6):671–8.
3. Bagis N, Kolsuz ME, Kursun S, Orhan K. Comparison of intraoral radiography and cone-beam computed tomography for the detection of periodontal defects: an in vitro study. BMC Oral Health. 2015;15(1):1–8.
4. Eskandarloo A, Arabi R, Bidgoli M, Yousefi F, Poorolajal J. Association between marginal bone loss and bone quality at dental implant sites based on evidence from cone beam computed tomography and periapical radiographs. Contemp Clin Dent. 2019;10(1):36–41.
5. Razavi T, Palmer RM, Davies J, Wilson R, Palmer PJ. Accuracy of measuring the cortical bone thickness adjacent to dental implants using cone beam computed tomography. Clin Oral Implants Res. 2010;21(7):718–25.
6. de Azevedo-Vaz SL, de Faria Vasconcelos K, Neves FS, Melo SLS, Campos PSF, Haiter Neto F. Detection of periimplant fenestration and dehiscence with the use of two scan modes and the smallest voxel sizes of a cone-beam computed tomography device. Oral Surg Oral Med Oral Pathol Oral Radiol. 2013;115(1):121–7.
7. Scarfe WC, Farman AG, Sukovic P. Clinical applications of cone-beam computed tomography in dental practice. J Can Dent Assoc. 2006;72(1):75-80.
8. Kolsuz M, Bagis N, Orhan K, Avsever H, Demiralp KÖ. Comparison of the influence of FOV sizes and different voxel resolutions for the assessment of periodontal defects. Dentomaxillofacial Radiol. 2015;44(7):20150070.
9. Xi Y, Jin Y, De Man B, Wang G. High-kVp assisted metal artifact reduction for X-ray computed tomography. IEEE Access. 2016;4:4769–76.
10. Parrone MT, Bechara B, Deahl ST II, Ruparel NB, Katkar R, Noujeim M. Cone beam computed tomography image optimization to detect root fractures in endodontically treated teeth: an in vitro (phantom) study. Oral Surg oral Med oral Pathol oral Radiol. 2017;123(5):613–20.
11. Schriber M, Yeung AWK, Suter VG, Buser D, Leung YY, Bornstein MM. Cone beam computed tomography artefacts around dental implants with different materials influencing the detection of peri-implant bone defects. Clin Oral Implants Res. 2020;31(7):595–606.
12. Kurt MH, Bağış N, Evli C, Atakan C, Orhan K. Comparison of the different voxel sizes in the estimation of peri-implant fenestration defects using cone beam computed tomography: an ex vivo study. Int J Implant Dentistry. 2020;6:1–11.
13. Kamburoğlu K, Kolsuz E, Murat S, Eren H, Yüksel S, Paksoy C. Assessment of buccal marginal alveolar peri-implant and periodontal defects using a cone beam CT system with and without the application of metal artefact reduction mode. Dentomaxillofacial Radiol. 2013;42(8):20130176.
14. Costa J, Mendes J, Salazar F, Pacheco J, Rompante P, Câmara M. Analysis of peri-implant bone defects by using cone beam computed tomography (CBCT): an integrative review. Oral Radiol. 2023;39(3):455–66.
15. Bagis N, Kurt MH, Evli C, Camgoz M, Atakan C, Peker Ozturk H, et al. Evaluation of a metal artifact reduction algorithm and an adaptive image noise optimization filter in the estimation of peri-implant fenestration defects using cone beam computed tomography: an in-vitro study. Oral Radiol. 2022;38(3):325–35.
16. Sawicki P, Zawadzki PJ, Regulski P, Zawadzki P, Regulski PA. The impact of cone-beam computed tomography exposure parameters on peri-implant artifacts: a literature review. Cureus. 2022;14(3):1–11.
17. Bechara B, McMahan CA, Nasseh I, Geha H, Hayek E, Khawam G, et al. Number of basis images effect on detection of root fractures in endodontically treated teeth using a cone beam computed tomography machine: an in vitro study. Oral Surgery, Oral Medicine, Oral Pathology and Oral Radiology. 2013;115(5):676–81.
18. Bechara B, Alex McMahan C, Moore W, Noujeim M, Teixeira F, Geha H. Cone beam CT scans with and without artefact reduction in root fracture detection of endodontically treated teeth. Dentomaxillofacial Radiol. 2013;42(5):20120245.
19. Freire BB, Wanderley VA, Câmara JVF, Santos LA, Ferrari CR, Araujo TT, et al. Effect of a metal artifact reduction algorithm on dehiscence and fenestration detection around zirconia implants with cone beam computed tomography. Oral Medicine, Oral Pathology and Oral Radiology: Oral Surgery. 2024;138(2):316–23.
20. Shahmirzadi S, Sharaf RA, Saadat S, Moore WS, Geha H, Tamimi D, et al. Assessment of the efficiency of a pre-versus post-acquisition metal artifact reduction algorithm in the presence of 3 different dental implant materials using multiple CBCT settings: an in vitro study. Imaging Sci Dentistry. 2021;51(1):1–7.
21. Kamburoğlu K, Murat S, Kılıç C, Yüksel S, Avsever H, Farman A, et al. Accuracy of CBCT images in the assessment of buccal marginal alveolar peri-implant defects: effect of field of view. Dentomaxillofacial Radiol. 2014;43(4):20130332.
22. Hilgenfeld T, Juerchott A, Deisenhofer UK, Krisam J, Rammelsberg P, Heiland S, et al. Accuracy of cone-beam computed tomography, dental magnetic resonance imaging, and intraoral radiography for detecting peri-implant bone defects at single zirconia implants—An in vitro study. Clin Oral Implants Res. 2018;29(9):922–30.
23. Rodrigues Pinheiro L, Scarfe WC, de Oliveira Sales MA, Gaia BF, Gonzalez Cortes AR, Paraiso Cavalcanti MG. Effectiveness of Periapical Radiography Versus Cone Beam Computed Tomography with different kilovoltage settings in the detection of chemically created peri-implant bone defects: an in Vitro Study. Int J Oral Maxillofacial Implants. 2017;32(4):741–50.

24. Schwindling FS, Hilgenfeld T, Weber D, Kosinski MA, Rammelsberg P, Tasaka A. In vitro diagnostic accuracy of low-dose CBCT for evaluation of Peri-implant bone lesions. Clin Oral Implants Res. 2019;30(12):1200–8.
25. Steiger-Ronay V, Krcmaric Z, Schmidlin PR, Sahrmann P, Wiedemeier DB, Benic GI. Assessment of Peri-implant defects at titanium and zirconium dioxide implants by means of periapical radiographs and cone beam computed tomography: an in-vitro examination. Clin Oral Implants Res. 2018;29(12):1195–201.

Publisher's Note